



Article

Facile Synthesis and Surface Characterization of Titania-Incorporated Mesoporous Organosilica Materials

Chamila Gunathilake ^{1,*}, Chandrakantha Kalpage ¹, Murthi Kadanapitiye ¹,
Rohan S. Dassanayake ², Amanpreet S. Manchanda ³ and Mahinda Gangoda ⁴

¹ Department of Chemical and Processing Engineering, Faculty of Engineering, University of Peradeniya, Kandy 20400, Sri Lanka

² Department of Chemistry, Ithaca College, Ithaca, NY 14850, USA

³ Department of Chemistry, California State University Stanislaus, One University Circle, Turlock, CA 95382, USA

⁴ Department of Chemistry and Biochemistry, Kent State University, Kent, OH 44242, USA

* Correspondence: chamilag@pdn.ac.lk; Tel.: +947-1831-1117

Received: 4 June 2019; Accepted: 15 July 2019; Published: 1 August 2019



Abstract: Titania-incorporated organosilica-mesostructures (Ti-MO) were synthesized using tris [3-(trimethoxysilyl)propyl]isocyanurate, tetraethylorthosilicate as silica precursors, and titanium isopropoxide as the titanium precursor via a co-condensation method in the presence of the triblock copolymer, Pluronic P123. The triblock copolymer was completely removed by extraction with a 95% ethanol solution, followed by a thermal treatment at 350 °C under flowing nitrogen without decomposing isocyanurate bridging groups. The molar ratio of titanium to silica in the mesostructures was gradually changed by increasing the amount of tetraethylorthosilicate in the initial reaction mixture. Our synthesis strategy also allowed us to tailor both adsorption and structural properties, including a well-developed specific surface area, high microporosity, and large pore volume. A portion of the samples was thermally treated at 600 °C to remove both the block copolymer and bridging groups. The thermal treatment at 600 °C was used to convert the amorphous titania into a crystalline anatase form. The Ti-MO materials were characterized using a N₂ adsorption desorption analysis, thermogravimetric analysis (TGA), solid state nuclear magnetic resonance (NMR), transmission electron microscope (TEM), and X-ray powder diffraction (XRD). CO₂ adsorption studies were also conducted to determine the basicity of the Ti-MO materials. The effect of the surface properties on the CO₂ sorption was also identified.

Keywords: mesoporous organosilica; one-pot synthesis; bridging groups; extraction-calcination; microporous volume; CO₂ adsorption

1. Introduction

The synthesis of organic–inorganic materials using organosilica precursors has generally been studied through two main pathways: (1) post-synthesis functionalization (post-grafting), and (2) co-condensation (one-pot synthesis) [1]. The post-grafting pathway utilizes the template free mesoporous silica with reactive alkoxyorganosilane, whereas the one-pot synthesis involves the reaction of a template containing mesostructure with alkoxyorganosilane. Mesoporous organosilica (MO) materials have recently become an area of particular interest in the field of nanoscience due to their tunability of adsorption and structural properties. MO materials allow high loading of organic functionalities into the silica structure, giving tunable adsorption properties such as specific surface area, pore volume, pore width, and well-ordered mesoporous structure. Because of these features, MO

materials have been widely used in applications, including adsorption, catalysis, chromatography, nonlinear optics, and drug delivery [1–7]. Different types of metal oxides, including titanium dioxide (TiO_2), vanadium oxides (VO_x), chromium oxides (Cr_xO_x), aluminum oxide (Al_2O_3), iron oxides (Fe_xO_y), magnesium oxide (MgO), zinc oxide (ZnO), and zirconium oxide (ZrO_2), have also been introduced into the mesopores to improve the catalytic properties of MO materials [8–13]. These metal oxides-incorporated MO materials exhibit distinctive catalytic properties as compared to traditional catalysts. Among those metal oxides, titanium-containing MO materials (Ti-MO) prepared using either co-condensation or post grafting strategies have been intensively investigated in catalytic/photocatalytic related applications [8–10,14–17]. For instance, Ti grafted mesoporous MCM-41 was studied by Gianotti and co-workers for catalytic applications [9]. Hu and co-workers synthesized chromium oxide on silica materials for a selective photocatalytic oxidation of carbon monoxide with oxygen [10]. Chao and co-workers studied various metal oxides (Al, Ti, V, Zr, and Fe oxides) incorporated silica frameworks for the cumene-cracking reaction [11]. Vinu and co-workers synthesized ordered Mg-Al-MCM-41 materials and checked their catalytic performance on the isopropylation reaction [12]. Alba and co-workers worked on Ti incorporated mesoporous silica (MCM 41) materials. They investigated the location and coordination of titanium species inside the silica matrix [13].

Titanium-incorporated MCM-48 and SBA-15 materials were studied by Morey and co-workers. They introduced titanium species into MCM-48 and SBA-15 by hydrothermal and post-synthesis grafting and characterized the properties of the resulting materials [14]. Ti-MO materials have also been reported as photocatalysts for the decomposition of organic dyes [18], oxidation of olefins [19,20], and reduction of CO_2 [21]. Titania-incorporated ZSM-12, ZSM-48, and Zeolite β materials have also been studied for the selective oxidation of alkanes, hydroxylation of phenols, and epoxidation of alkenes using peroxide as an oxidant [22–24]. Kapoor and co-workers synthesized titanium-incorporated mesoporous aluminophosphate materials and used them as a catalyst for the epoxidation of alkenes [25]. They also synthesized hydrophobic Ti-MO materials as a very efficient catalyst in the epoxidation of α -Pinene [26], epoxidation of propene to propene oxide [27], and ammoxidation of ketone to oxime [28]. Ritterskamp and co-workers reported the use of titanium anchored silanol groups for liquid phase oxidation [29]. Typically, the catalytic/photocatalytic properties of Ti-Si composites depend on several factors, including the amount of incorporated titanium, crystalline form of titanium in the silica framework, and the hydrophobicity of the surface.

The current study reports the facile synthesis and surface characterization of titanium-incorporated mesoporous organosilica (Ti-MO) materials with or without isocyanurate bridging groups. Here, we also investigate the surface properties of Ti-MO materials by changing the Ti:Si ratio and calcination temperatures.

2. Experimental Section

2.1. Materials

Tris [3-(trimethoxysilyl)propyl]isocyanurate (ICS), and tetraethylorthosilicate (TEOS) were purchased from Gelest Inc. (Morrisville, PA, USA). PluronicP123 ($\text{EO}_{20}\text{PO}_{70}\text{EO}_{20}$) triblock copolymer was donated by the BASF Corporation (Flortham Park, NJ, USA). HCl (37%), ethanol (95%), and titanium isopropoxide (TiPO) were purchased from Fisher Scientific (Pittsburgh, PA, USA). Deionized water (DW) was obtained using the in-house Ionpure Plus 150 service deionization ion-exchange purification system. All reagents were analytical grade and used with no further purification.

2.2. Preparation

The recipe used for the preparation of Ti-MO composite mesostructures was reported elsewhere by Melero et al. [30]. In a typical synthesis, 4.0 g of Pluronic P123 ($\text{EO}_{20}\text{PO}_{70}\text{EO}_{20}$) was mixed with 0.5 M HCl (125 mL) and was completely dissolved within 2 h under rapid stirring at room temperature. The mixture was then heated to 40 °C and a specified amount of Titanium isopropoxide (TiPO) was added

and stirred for 3 h. Next, a predetermined amount of Tris [3-(trimethoxysilyl)propyl]isocyanurate (ICS) and tetraethylorthosilicate (TEOS) was added to the mixture and further stirred at 40 °C for 20 h. Subsequently, the solution was hydrothermally treated in an oven at 100 °C for 24 h. The resulting solution was added to a 200 mL round bottom flask containing 95% of ethanol and refluxed at 40 °C for 24 h. Afterward, the solution was transferred to a Pyrex Petri dish and dried at 120 °C for 24 h and heated in a horizontal quartz tube furnace at 350 °C for 2 h in flowing N₂ with a heating rate of 2 °C/min. Another portion of the dried samples was thermally heated in a horizontal quartz tube furnace oven at 600 °C for 6 h in flowing N₂ with a heating rate of 1 °C/min.

The total amount of Ti moles was kept constant at 0.011. The silicon moles were taken as a percentage of the total titanium moles. The resulting samples were labeled with the starting prefixes Ti, I, and TS for the TiPO, ICS, and TEOS precursors, respectively, which were used in the initial synthesis mixture. For instance, Ti-Ix is donated to the samples containing ICS as a silica precursor; whereas Ti-Ix-TSy was donated to the samples containing ICS and TEOS as silica precursors. In both cases, TiPO was used as the titanium precursor. Ti-Ix contains x% of silicon moles (w.r.t total titanium moles) originating from ICS, whereas Ti-Ix-TSy contains x and y% of silicon moles originating from both ICS and TEOS precursors, respectively. For instance, Ti-I10-TS50 indicates 10% (10% w.r.t total titanium moles (0.011) = 0.0011 moles) of ICS and 50% (50% w.r.t total titanium moles (0.011) = 0.0055 moles) of TEOS. All as-synthesized samples were donated with the # symbol. The as-synthesized samples were subjected to the extraction step, followed by the thermal treatment in flowing nitrogen at 350 and 600 °C. The samples with and without the * notation represent the thermal treatment at 600 and 350 °C, respectively. For the purpose of comparison, another set of samples was synthesized with TiPO using the similar recipe described above, but without adding any silica precursors. Those samples were also thermally treated at 350 and 600 °C and denoted with Ti[§] and Ti*, respectively. Table 1 summarizes the sample labeling with the specific notations, sample precursors and conditions under which the samples were synthesized.

Table 1. Summary of the notations, precursors, and conditions of the synthesized materials.

Sample Notation	Precursors	Condition	TiPO Moles	ICS Moles (x)	TEOS Moles (y)
Ti [§]	TiPO	Extracted-Calcined at 350 °C	0.011	-	-
Ti*	TiPO	Calcined at 600 °C	0.011	-	-
Ti-Ix-TSy [#]	ICS, TEOS, TiPO	As-Synthesized	0.011	0.011 (x)/100	0.011 (y)/100
Ti-Ix	ICS, TiPO	Extracted-Calcined at 350 °C	0.011	0.011 (x)/100	-
Ti-Ix-TSy	ICS, TEOS, TiPO	Extracted-Calcined at 350 °C	0.011	0.011 (x)/100	0.011 (y)/100
Ti-Ix-TSy*	ICS, TEOS, TiPO	Calcined at 600 °C	0.011	0.011 (x)/100	0.011 (y)/100

TiPO-Titanium isopropoxide, Tris [3-(trimethoxysilyl)propyl]isocyanurate (ICS), tetraethylorthosilicate (TEOS).

2.3. Measurements

Nitrogen adsorption isotherms were collected at −196 °C on an ASAP 2010 volumetric analyzer (Micromeritics, Inc., Norcross, GA, USA). All samples were degassed under vacuum at 110 °C for 2 h [31–34] prior to the adsorption measurements.

High-resolution thermogravimetric measurements were recorded on a TGA Q-500 analyzer (TA Instruments, Inc., New Castle, DE, USA). The thermogravimetric (TG) profiles were analyzed from 25 °C up to 800 °C in flowing nitrogen with a heating rate of 10 °C/min using the High Resolution TGA™ (Hi-Res™ TGA). The weight of each analyzed sample was typically in the 5–20 mg range. The TG profiles were used to obtain information about the extent of the template removal [31–34].

Powder Wide angle X-ray diffraction (XRD) measurements were performed using an X'Pert PRO MPD multipurpose diffractometer (PANalytical, Inc., Westborough, MA, USA) with a Cu K α radiation (0.15406 nm) at room temperature from 20.0° to 80.0°. The measurements were conducted using a voltage of 45 kV, a current setting of 40 mA, a step size of 0.020, and count times of 4 s. Microscope glass slides were used as sample supports for all samples [34].

A quantitative estimation of C and N (%) was obtained by CHNS analysis using a LECO model CHNS-932 elemental analyzer (St. Joseph, MI, USA) [31–34].

Transmission electron microscopy (TEM) images were obtained on a FEI Tecnai G2 F20 microscope. The energy dispersive X-ray spectroscopy (EDX) data were recorded by using an integrated scanning TEM (STEM) unit with an attached EDAX spectrometer. Prior to the TEM analysis, the sample powders were dispersed in ethanol by moderate sonication at concentrations of ~5 wt.%. A Lacy carbon coated, 200-mesh, copper TEM grid was dipped into the sample suspension and then dried under vacuum at 80 °C for 12 h [31–34].

2.4. Solid-State NMR

All NMR spectra were recorded on a 9.4 T using Bruker Avance (III) 400WB NMR spectrometer (Bruker Biospin Corporation, Billerica, MA, USA) with a MAS triple resonance probe head and zirconia rotors (4 mm in diameter).

^1H - ^{29}Si cross polarization (CP) MAS NMR spectra were recorded at 79.49 MHz for ^{29}Si and 400.13 MHz for ^1H . The MAS rate was 5 KHz. For ^1H , the $\pi/2$ pulse length was 4.5 μs , and the pulse delay was 3.0 s. A two pulse phase modulated TPPM15 decoupling sequence was used during the acquisition. The ^{29}Si chemical shifts were referenced to TMS (0 ppm). ^1H - ^{13}C CP-MAS NMR spectra were acquired at 400.13 MHz for ^1H and 100.63 MHz for ^{13}C . The MAS rate was 5 KHz. For ^1H , the $\pi/2$ pulse length was 3.5 μs , and the pulse delay was 2.0 s. A TPPM20 ^1H decoupling sequence was used during the acquisition. The ^{13}C chemical shifts were referenced to p-dioxane 66.6 ppm [31–34]. The contact time for ^1H - ^{29}Si CP-MAS NMR and ^1H - ^{13}C CP-MAS NMR is around 2–10 milli seconds (ms).

2.5. Calculations

The Brunauer-Emmett-Teller specific surface area (SBET) for the samples studied was calculated from N_2 adsorption isotherms in the relative pressure range of 0.05–0.2. The single-point pore volumes (V_{sp}) were estimated from the amounts adsorbed at a relative pressure of ~0.98. The pore size distributions (PSD) were calculated using the adsorption branches of nitrogen adsorption-desorption isotherms by employing the improved KJS method calibrated for cylindrical pores [35]. The pore width (W_{max}) was obtained at the maximum of the PSD curve.

2.6. Test of Basic Properties of Materials Using CO_2 Adsorption Measurement

The basicity of the materials was determined by CO_2 adsorption measurements for all samples studied, as described below:

The CO_2 adsorption onto the Ti-MO samples was performed in the pressure range up to 1 atm using ASAP 2020 volumetric adsorption analyzers (Micromeritics, Inc., Norcross, GA, USA) at 25 °C under ultrahigh purity (99.99%) CO_2 . Prior to the analysis, the samples were outgassed at 110 °C for 2 h under vacuum [31–34].

3. Results and Discussion

3.1. Properties of Ti-MO Samples Prepared at Different Synthesis Conditions

High-resolution thermogravimetry (TG) and differential thermogravimetry (DTG) profiles were used to study the thermal stability of the selected Ti-MO samples. The TG and DTG profiles of the Ti-I10-TS10[#], Ti-I10-TS10, and Ti-I10-TS10* composites are shown in Figure 1. As shown in the DTG profiles, the as-synthesized Ti-I10-TS10[#] sample exhibits three main decomposition peaks at

the temperature ranges of 20–120 °C, 170–350 °C, and 400–550 °C, corresponding to the removal of physically adsorbed water, decomposition of triblock copolymer template, and decomposition of isocyanurate bridging groups, respectively. The partially reduced peak appeared in the DTG profile of the extracted samples at 200–300 °C (data not shown) indicates that the extraction is not sufficient to remove the block copolymer template from the Ti-MO mesostructure. Thus, all extracted samples were further subjected to calcination at 350 °C to completely remove the block copolymer template from the studied mesostructures. Note that the peaks correspond to the decomposition of the block copolymer and isocyanurate bridging groups appear in the temperature range of 170–350 °C, and 400–550 °C, respectively. Thus, an additional heat treatment at 350 °C in flowing nitrogen facilitates the complete removal of the remaining polymer template without any decomposition of the isocyanurate bridging groups. The template peak visible at 200–300 °C disappeared after calcination (see Figure 1, DTG profile of Ti-I10-TS10). The unchanged peak centered at 450 °C results from the high thermal stability of the titanium-incorporated isocyanurate bridging groups containing materials. The DTG profiles of the samples that were thermally treated at 350 and 600 °C also exhibit a single peak at about 100 °C, which is due to the removal of physically adsorbed water. The disappearance of characteristic decomposition peaks of the sample Ti-I10-TS10* at 200–350 °C and 400–500 °C indicates the successful removal of both the block copolymer and bridging groups.

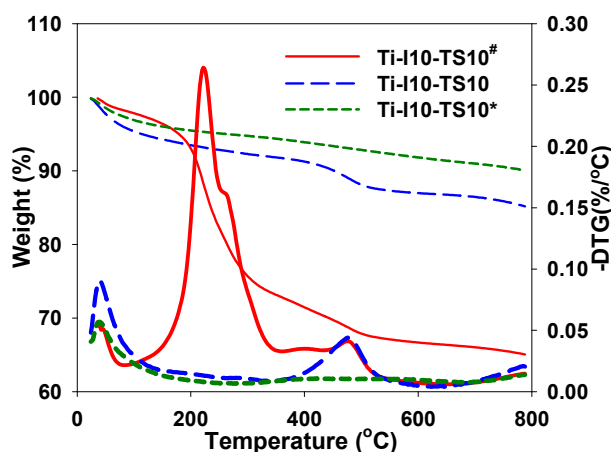


Figure 1. The TG and DTG curves for the as-synthesized, extracted and extracted calcined (350 and 600 °C) titania-silica composites.

Figure 2A,C and Figure 3A show the nitrogen adsorption-desorption isotherms measured at -196 °C of the studied Ti-MO samples. The corresponding PSD curves exhibited in Figure 2B,D and Figure 3B (right panels) were calculated from the adsorption branch of the aforementioned isotherms [31]. These isotherms are typically used to evaluate the effect of different synthesis conditions on the structural parameters of the Ti-MO materials, such as the specific surface area, total pore volume, pore size distribution, and pore width. Table 2 lists the structural parameters calculated for all isotherms. These isotherms can be considered as type IV, with hysteresis loops that resemble a H1 type, according to the IUPAC classification. The type IV isotherms with a hysteresis loop are attributed to the mesoporous materials. As can be seen from Figure 2 (left panel), the shapes of the isotherm curves and the corresponding PSD curves change gradually for the Ti-MO samples studied from Ti-I5-TS5 to Ti-I5-TS5, Ti-I10-TS10, Ti-I50-TS50, and Ti-I100. All extracted and calcined (350 °C) samples show a broad PSD.

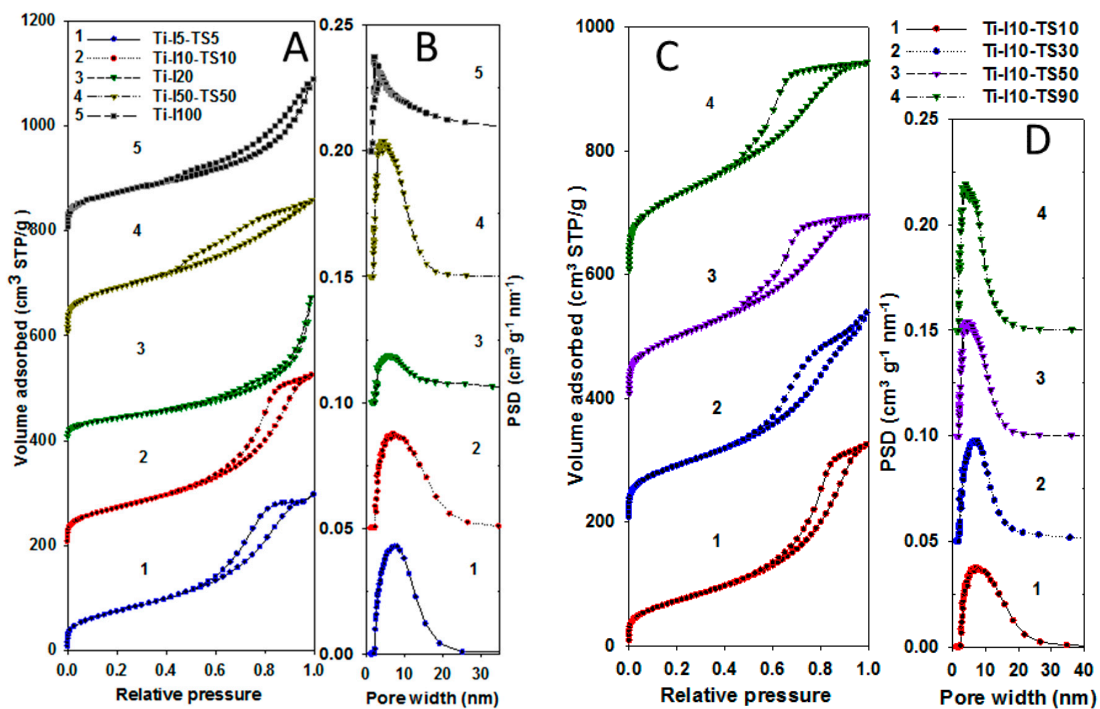


Figure 2. Left: (A) N₂ adsorption isotherms (left panel) and (B) the corresponding PSD curves for the Ti-I_x-TS_x (x = 5, 10, 50) and Ti-I_x (x = 20, 100) samples. Right: (C) N₂ adsorption isotherms (left panel) and (D) the corresponding PSD curves for the Ti-I10-TS_x samples thermally treated at 350 °C (All isotherms and PSD are shifted by a multiple of 200 cm³ STP/g and of 0.05 cm³ g⁻¹ nm⁻¹, respectively).

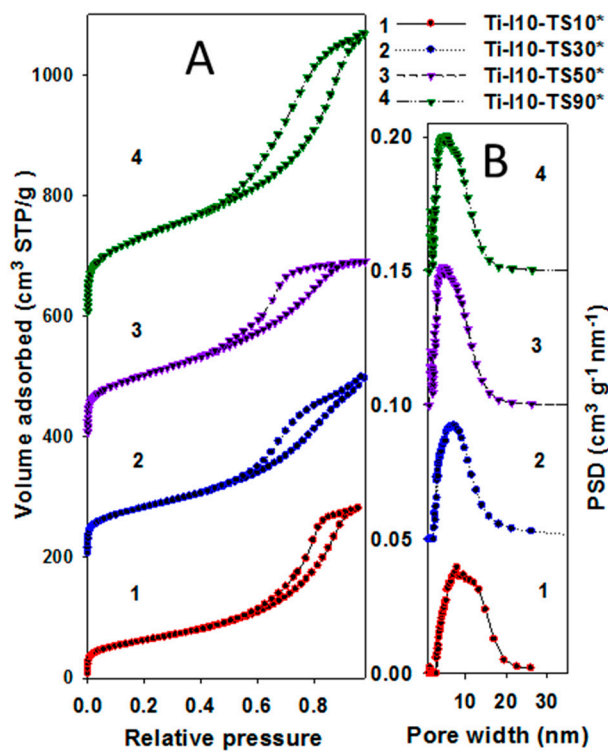


Figure 3. (A) N₂ adsorption isotherms and (B) the corresponding PSD curves for the Ti-I10-T_x* samples thermally treated at 600 °C (All isotherms and PSD are shifted by multiple of 200 cm³ STP/g and 0.05 cm³ g⁻¹ nm⁻¹, respectively).

Table 2. Structural parameters for the studied Ti-MO samples.

Isotherm	V_{sp} (cm^3/g)	V_{mi} (cm^3/g)	$S_{BET}/(\text{m}^2/\text{g})$	W_{max}/nm	N (mmol/g)	C (mmol/g)	Initial Ti/Si Ratio
Ti-I5-TS5	0.45	0.01	275	7.6	0.35	7.52	10:1
Ti-I10-TS10	0.50	0.01	264	7.3	0.65	8.38	10:2
Ti-I20	0.40	0.01	160	5.8	1.09	8.42	10:2
Ti-I50-TS50	0.39	0.04	334	4.0	1.80	13.90	10:10
Ti-I100	0.44	0.03	269	3.2	3.42	18.69	10:10
Ti [§]	0.36	0.01	144	9.2	-	-	-
Ti-I10-TS10	0.50	0.01	264	7.3	0.65	8.38	10:2
Ti-I10-TS30	0.51	0.02	332	7.3	0.60	7.21	10:4
Ti-I10-TS50	0.46	0.03	371	5.6	0.59	9.06	10:6
Ti-I10-TS90	0.53	0.05	475	4.8	0.52	9.88	10:10
Ti*	0.36	0.01	111	11.6	-	-	-
Ti-I10-TS10*	0.43	0.01	225	8.0	0.17	5.44	10:2
Ti-I10-TS30*	0.46	0.01	300	7.3	0.14	4.69	10:4
Ti-I10-TS50*	0.45	0.03	373	5.0	0.15	6.40	10:6
Ti-I10-TS90*	0.73	0.04	487	4.6	0.15	6.29	10:10

V_{sp} : single point pore volume calculated at the relative pressure of 0.98; S_{BET} : specific surface area calculated from the adsorption data in the relative pressure range of 0.05–0.20; V_{mi} : volume of fine pores (micropores and small mesopores below 3 nm) calculated by integration of the PSD curve up to 3 nm; W_{max} : pore width calculated at the maximum of PSD, using the improved KJS method; The concentration of N and C in the Ti-MO mesostructures was based on N and C% obtained by elemental analysis. TiPO: Titanium isopropoxide, ICS: Tris [3-(trimethoxysilyl)propyl]isocyanurate, TEOS: tetraethylorthosilicate.

As can be noted from Table 2, the structural parameters of the Ti-I20 and Ti-I100 samples, including the specific surface area, pore volume, and pore size, decreased with increasing amounts of isocyanurate bridging groups in the framework. Despite the similar molar percentage of silicon in the initial reaction mixture for Ti-I50-TS50 and Ti-I100, the Ti-I50-TS50 samples possess better structural parameters as compared to that of the Ti-I100 sample (see Table 2). These results may be attributed to efficient cross-linking between tetraethylorthosilicates that occurred during the hydrolyzation followed by the condensation. The structural collapse and shrinkage of bulky isocyanurate groups under thermal treatment may also possibly decrease the structural parameters. This result further reflects that the structural parameters of the studied Ti-MO samples are mainly dependent on the loading of bulky organic groups. Moreover, the condensation/evaporation steps became broader with increasing concentration of ICS in the initial reaction mixture, which suggests the gradual shrinkage of the mesoporous structure (Figure 2A,B). A comparison of the isotherms is shown in Figure 2A, which indicates that increasing the amount of reactive organosilane influences the shape of adsorption isotherms, except for the samples with a low ICS content in the initial reaction mixture. For instance, the hysteresis loop observed for the Ti-I5-TS5 and Ti-I10-TS10 samples is H1, because both the adsorption and desorption branches are almost parallel to each other and perpendicular to the relative pressure axis, whereas the interpretation of the hysteresis loops for Ti-I100 is more difficult, although it resembles the H1-type. This may be caused by the geometrical constrictions resulting from the presence of high amounts of bulky isocyanurate bridging groups in the framework. Thus, the experiment is further continued by keeping a constant percentage (10%) of Si moles originating from ICS, while progressively

increasing the amount of Si moles originating from TEOS in the initial reaction mixture in order to obtain tailorable structural parameters.

A series of Ti-I10-TSX ($X = 10, 30, 50, 90$) samples produced by varying the amount of TEOS present in the initial reaction mixture, show type IV isotherms with a well-resolved H_2 hysteresis loop (see Figure 2C). A gradual change in the adsorption properties was observed for the samples ranging from the Ti-I10-TS10 to Ti-I10-TS90 samples. The presence of micropores contributes to an increased specific surface area, reaching values from 264 to 475 m^2/g accordingly (see Table 2). In contrast, the mesopore size of the Ti-I10-TS90 sample is smaller than that of the Ti-I10-TS10; Ti-I10-TS90 has a mesopore size of about 4.85 nm, as estimated at the maximum of PSD, whereas the mesopore size of Ti-I10-TS10 is 7.3 nm. The thermal treatment at 600 °C was conducted to remove both the Pluronic P123 block copolymer and isocyanurate bridging groups of the materials studied and to further study the deviation of their surface properties and their effects on the catalytic activity. However, the Ti-I10-TSX* ($X = 10, 30, 50, 90$) samples exhibit no significant change in the shape of the isotherms, their corresponding PSD curves and the structural parameters, as compared to the corresponding samples thermally treated at 350 °C (see Figure 3 and Table 2). For instance, the Ti-I10-TS50 sample calcined at 350 °C exhibits a surface area and pore volume of about 371 m^2/g and 0.46 cm^3/g . Upon thermal treatment at 600 °C, the Ti-I10-TS50* sample exhibits a surface area and pore volume of about 373 m^2/g and 0.45 cm^3/g , respectively (see and compare Ti-I10-TS50 and Ti-I10-TS50* in Figures 2 and 3, and in Table 2).

CHNS analysis was conducted to determine the amount of carbon and nitrogen in the Ti-Si matrix. As shown in Table 1, from Ti-I5-TS5 to Ti-I100, the amount of ICS is increased with respect to TEOS, and thus the amount of C (mmol/g) and N (mmol/g) are gradually increased. For all samples calcined at 350 °C, a block co-polymer was decomposed and was expected to have a constant amount of C and N (mmol/g), since only 10% of ICS was incorporated into the silica matrix. For instance, Ti-I10-TS30 and Ti-I10-TS50, respectively, have 0.60 and 0.59 mmol/g of N. Upon calcination at 600 °C, although it is expected to have no ICS, in practice, it is possible to have a reasonable amount of C and N that could be embedded in the silica matrix. Therefore, the CHNS analysis displays both N and C for the samples calcined at 600 °C, which could be due to the presence of small amounts of block-co polymers and bridging groups remain in residues.

Wide angle powder X-ray diffraction measurements were employed to identify the crystalline properties of the studied materials. Figure 4 shows the XRD patterns of the Ti-I10-TS10 and Ti-I10-TSX* ($x = 10, 30, 50, 90$) materials. As shown in Figure 4, the thermal treatment of the titania-silica composite at 350 °C shows characteristic peaks at $2\theta = 24.5, 29.3, 34.2, 38.0, 48.0, 54.1,$ and 62.8 , and thus represents the anatase phase (ICDD PDF file # 01-073-1764). However, calcination at 600 °C dramatically increases the degree of crystallization. All of the Ti-I10-TSX* samples possess a considerably higher degree of crystallinity, attributed to the rutile form of TiO_2 . Peaks appearing at $2\theta = 25.5, 38.3, 47.8, 63.1, 69.3,$ and 76.5 are attributed to the rutile phase (ICDD PDF# 01-087-0710). [13,14]. However, note that the samples calcined both at 350 and 600 °C are relatively broader and show a low degree of crystallinity Figure 5, which shows the TEM images of Ti-I10-TS50 and Ti-I10-TS50*, indicates an aggregation of small particles. It was proposed that such mesostructures are often useful over ordered structures for catalytic applications due to the branching, which subsequently enhances the accessibility of molecules to the active sites [13,14]. The energy dispersive X-ray (EDX) spectrum describes the elemental dispersion throughout the silica framework for the samples thermally treated at 350 °C (see Figure 6) and 600 °C (data not shown). The EDX spectrum was probed at six different places for each sample. Thus, the incorporation of titanium species into the silica matrix is evidently confirmed.

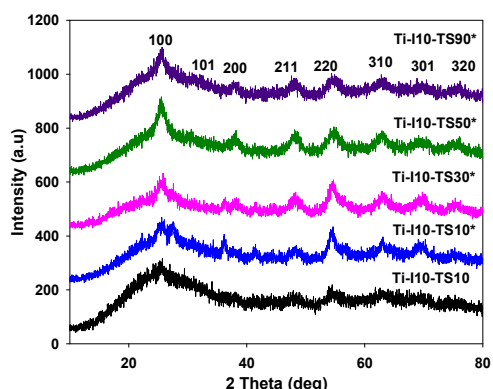


Figure 4. Wide angle XRD patterns for the Ti-I10-TS10 & Ti-I10-TSx* samples (x = 10, 30, 50, 90).

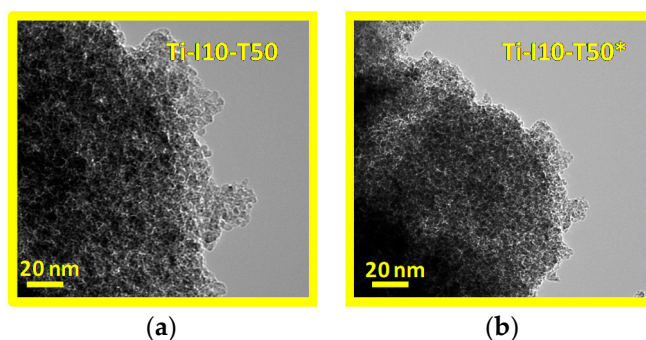


Figure 5. TEM images for the Ti-I10-TS50 (a) and Ti-I10-TS50* (b) samples.

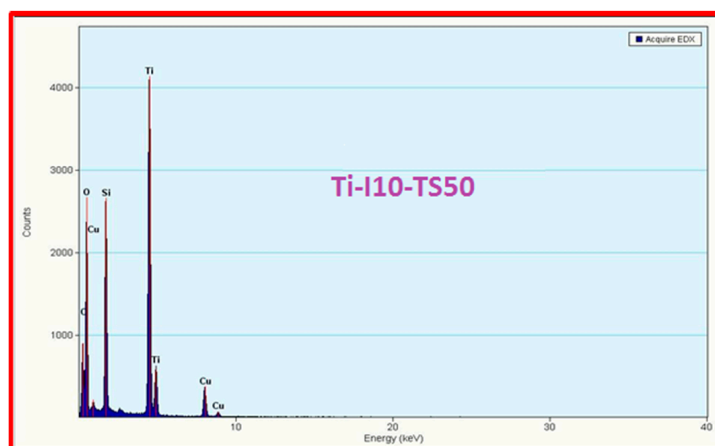


Figure 6. The EDX spectrum for the Ti-I10-TS50 sample.

The solid state NMR data identify the nature of siloxane bonds and the existence of isocyanurate bridging groups in the studied Ti-MO mesostructures. A ^{13}C NMR study is used to identify the incorporation of the isocyanurate group into the matrix. The ^1H - ^{13}C CP/MAS spectra for the Ti-I10-TSX (X = 10, 30, 50, 90) samples exhibit an identical chemical shift (δ). For instance, the Ti-I10-TS10 sample shows resonance peaks at ~ 10 and 21 ppm corresponding to the C atoms bonded to the Si atoms and C atoms in propyl linkages of isocyanurate bridging groups. C atoms directly attached to the embedded N atoms in the isocyanurate ring and isocyanurate bridging groups display peaks at 60 and 149.5 ppm (see Figure 7 [34,36,37]). The peak intensities of ^1H - ^{13}C CP-MAS NMR for the Ti-I10-TS10 and Ti-I10-TS90 samples are different. However, their relative peak positions corresponding to specific functional groups of isocyanurate are the same. In the NMR studies, the ICS:TEOS ratio changed from Ti-I10-TS10 to Ti-I10-TS90, and thus their peak intensities can be varied. However, the peak position

is characteristic for a given sample, and thus the ICS content (carbon) is the same for both samples, showing a similar spectral pattern and peak positions. Please note that TEOS could affect the peak intensity but not the position in which the peaks appear.

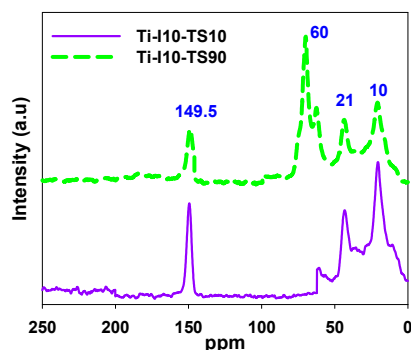


Figure 7. The ^1H - ^{13}C CP-MAS NMR spectra for the Ti-I10-TS10 and Ti-I10-TS90 samples.

^1H - ^{29}Si CP-MAS was employed to confirm the existence of Si in the matrix and how Si is bonded with other Si through oxygen. The ^1H - ^{29}Si CP-MAS NMR spectrum of the Ti-I10-TS10 sample shows two major resonance peaks at ~ -100 and -66 ppm (see Figure 8 [13,14,36]). Those peaks can be attributed to Q^3 species ($\text{Si}(\text{OSi})_3\text{OH}$)/($\text{Si}(\text{OSi})_3(\text{OTi})$) and T^3 species ($\text{R-Si}(\text{OSi})_2\text{OH}$)/ $\text{T}^3(\text{R-Si}(\text{OSi})_3)$. A shoulder peak at -90 ppm reflects the existence of Q^2 species ($\text{Si}(\text{OSi})_2(\text{OH})_2$)/($\text{Si}(\text{OSi})_2(\text{OH})(\text{OTi})$) in the studied Ti-MO mesostructures [13,14,34,36,37].

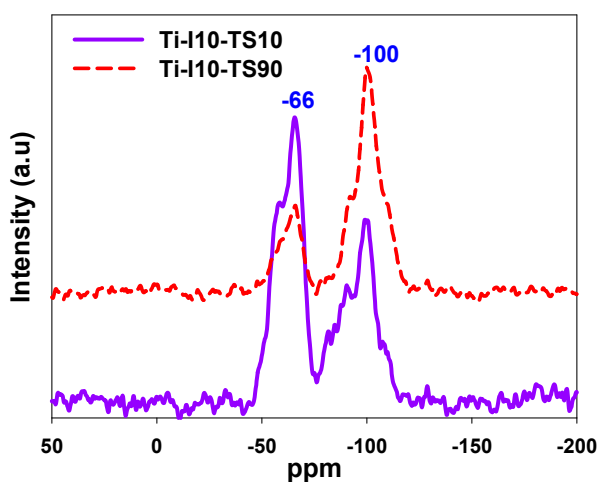


Figure 8. The ^1H - ^{29}Si -CP MAS NMR spectra for the Ti-I10-TS10 and Ti-I10-TS90 samples.

S_{BET} : specific surface area was calculated from the adsorption data in the relative pressure range of 0.05–0.20; The concentration of N in the Ti-MO mesostructures was determined based on the N% obtained by elemental analysis; n CO_2 : maximum number of moles of CO_2 adsorbed per gram of the sample; n^* CO_2 : number of moles of CO_2 adsorbed per unit surface area of sample; ASA: active surface area obtained from n CO_2 using $0.218 \text{ nm}^2/\text{molecule}$ average value of the cross-sectional area of CO_2 (reported by McClellan and Harnsberger in J. Colloid Interface Sci. 1967, 23, 577–599); $100 \times \text{ASA}/S_{\text{BET}}$ – percentage of active surface area. TiPO: Titanium isopropoxide, ICS: Tris [3-(trimethoxysilyl)propyl]isocyanurate, TEOS: tetraethylorthosilicate.

3.2. CO_2 Adsorption

The alkaline properties of the Ti-MO materials were investigated through acidic CO_2 sorption. The alkaline nature of the synthesized material depends substantially on synthesis conditions and surface

properties. Figures 9 and 10a,b show the comparison of the CO₂ adsorption isotherms measured at ambient conditions (298 K and 1 atm) for the series of studied Ti-MO samples. As can be seen from Table 3 and Figures 9 and 10a,b, the incorporation of a large amount of TEOS in the initial reaction mixture leads to an enhanced CO₂ uptake with a higher basicity, whereas the functionalization with a high amount of isocyanurate bridging group results in a decreased CO₂ uptake at 25 °C. The CO₂ adsorption at ambient temperature is usually governed through physisorption. It is noteworthy to mention that a higher CO₂ uptake for the Ti-I10-T90 and Ti-I10-T90* samples is due to their higher microporosities. This indicates the importance of microporosity for CO₂ adsorption at low temperatures and pressures. Surprisingly, samples with a higher nitrogen content show a relatively lower CO₂ uptake. CO₂ adsorption at low temperatures is mainly governed through physisorption, rather than chemisorption. The micropores volume responsible for physisorption and the N content is mostly important for chemisorption. Since our CO₂ sorption experiment was conducted at 25 °C, the amount of N percent has no effect on the CO₂ sorption but does have a significant effect on the microporous volume. A higher microporous volume attributes to a higher CO₂ sorption (compare Tables 2 and 3). The Ti-I20 and Ti-I100 samples display a CO₂ uptake of about 0.60 and 0.55 mmol/g, respectively. However, samples with higher molar percentages of Si, giving increased the microporous volume, and thus the Ti-Si composites (Ti-I10-TSx and Ti-I10-Tx*) show increased CO₂ uptakes with increasing micropore volume. The CO₂ uptake changes from 0.48 mol g⁻¹ for Ti-I10-T10* to 0.81 mol g⁻¹ for Ti-I10-T90*. Moreover, there are no visible differences in the CO₂ uptake between the Ti-I10-Ty samples and their corresponding Ti-I10-Ty* (y = 10, 30, 50, 90) samples, indicating the importance of a high surface area and microporosity, as compared to the role of nitrogen reactivity in ambient conditions. Despite their thermal treatment at either 350 or 600 °C, the active surface area (ASA) for the CO₂ adsorption increased with increasing molar percentage of Si in the studied Ti-Si composites (see Table 3). All Ti-I10-Ty and Ti-I10-Ty* (y = 10, 30, 50, 90) samples display over 19% active surface area (ASA) from the available specific surface area for CO₂ adsorption. The active surface area was also calculated based on the CO₂ sorption, which is dependent on the microporous volume, therefore having an inverse relationship with the nitrogen content.

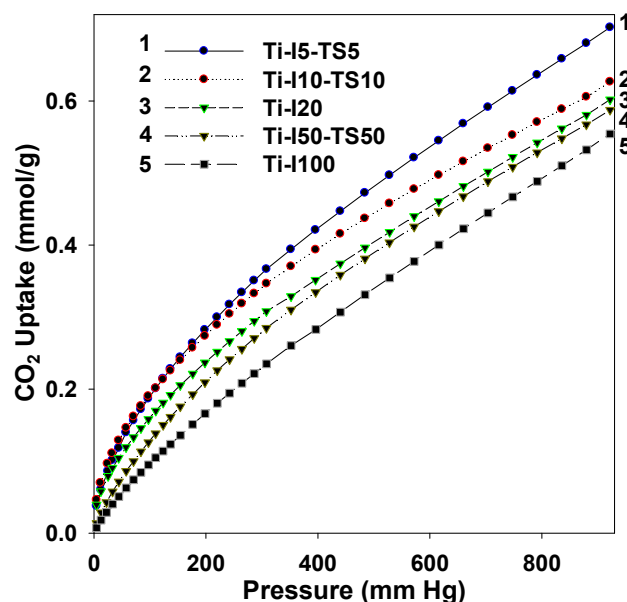


Figure 9. CO₂ sorption isotherms at 25 °C measured on Ti-Ix (x = 20, 100) and Ti-I10-TSx (x = 5, 10, 50).

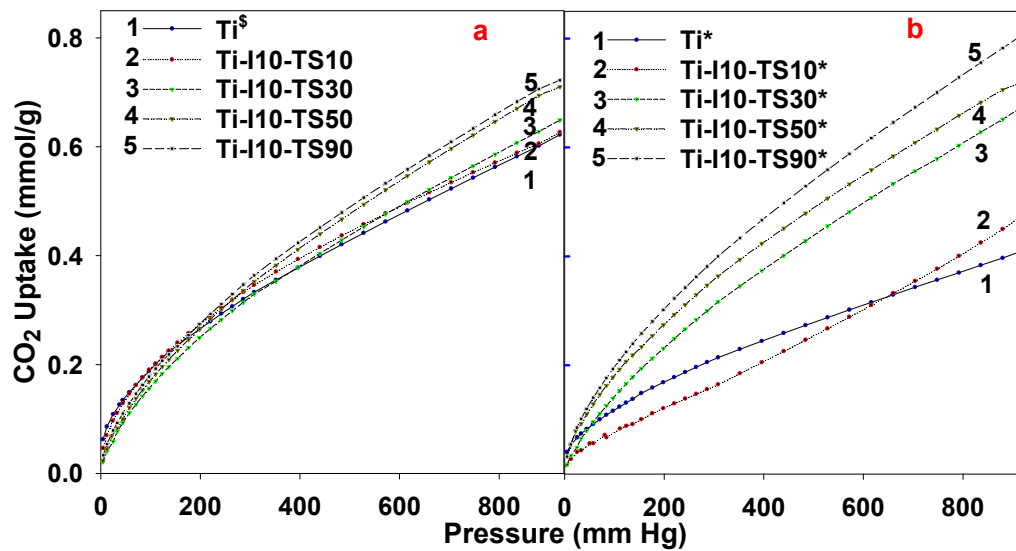


Figure 10. CO₂ sorption isotherms at 25 °C measured on the (a) Ti-I10-TS_x and (b) Ti-I10-TS_x* samples; (x = 10, 30, 50, 90).

Table 3. Structural parameters and CO₂ uptake values at 25 °C for the studied Ti-MO samples.

Sample	S _{BET} (m ² /g)	N (mmol/g)	n CO ₂ (mmol/g)	n*CO ₂ (μmol/m ²)	ASA (m ² /g)	100.ASA/S _{BET} (%)
Ti-I5-TS5	275	0.35	0.70	2.54	91.9	33.4
Ti-I10-TS10	264	0.65	0.63	2.38	82.7	31.3
Ti-I20	160	1.09	0.60	3.75	78.8	49.2
Ti-I50-TS50	334	1.80	0.59	1.76	77.4	23.2
Ti-I100	269	3.42	0.55	2.05	72.2	26.9
Ti ^S	144	-	0.62	4.30	81.4	56.5
Ti-I10-TS10	264	0.65	0.63	2.38	82.7	31.3
Ti-I10-TS30	332	0.60	0.64	1.93	84.0	25.3
Ti-I10-TS50	371	0.59	0.69	1.86	90.6	24.4
Ti-I10-TS90	475	0.52	0.72	1.52	94.5	19.9
Ti*	111	-	0.41	3.68	53.8	48.3
Ti-I10-TS10*	225	0.17	0.48	2.13	63.0	28.0
Ti-I10-TS30*	300	0.14	0.68	2.27	89.3	29.8
Ti-I10-TS50*	373	0.15	0.72	1.93	94.5	25.3
Ti-I10-TS90*	487	0.15	0.81	1.66	106.3	21.8

4. Conclusions

A series of Ti-incorporated isocyanurate bridging groups containing mesoporous organosilica materials (Ti-MO) were synthesized using a P123 block copolymer as a structure-directing agent via a co-condensation method by changing the composition of tris [3-(trimethoxysilyl)propyl]isocyanurate (ICS) and tetraethylorthosilicate (TEOS) precursors in the initial reaction mixture and thermally calcining them at 350 and 600 °C. The incorporation of the isocyanurate group was identified by the characteristic decomposition peak observed in thermogravimetric profile at 400–550 °C. The ¹³C NMR studies and ²⁹Si NMR studies further revealed the existence of isocyanurate groups and siloxane bonds, respectively. A significant change in the surface properties can be observed with varying Ti:Si

ratios. Increasing the amount of TEOS in the initial mixture resulted in enhanced structural properties, including high specific surface area and large mesopore volume, whereas those properties decreased upon high loading of the isocyanurate bridging groups. A wide angle XRD analysis revealed that all samples thermally treated at 350 °C were attributable to the anatase crystalline form of titania, while the samples thermally treated at 600 °C were ascribed to the rutile phase. Interestingly, the samples thermally heated at 600 °C exhibited higher basic properties in comparison to the similar samples thermally treated at 350 °C. Due to the low cost, environmentally benign nature and relatively easy synthesis route, Ti-MO materials show potential in catalytically-driven industrial processes, including oxidation, epoxidation, and hydroxylation.

Author Contributions: Formal analysis, C.G., M.K. and R.S.D.; Investigation, C.K., A.S.M. and M.G.; Methodology, C.G. and A.S.M.; Project administration, C.K. and M.K.; Resources, C.G. and M.G.; Validation, R.S.D.; Visualization, M.G.; Writing—original draft, C.G.; Writing—review & editing, C.G., C.K., R.S.D. and A.S.M.

Funding: This research received no external funding.

Acknowledgments: The TEM data were obtained at the (cryo) TEM facility at the Liquid Crystal Institute, Kent State University, supported by the Ohio Research Scholars Program Research Cluster on Surfaces in Advanced Materials. The authors thank Min Gao for the technical support with TEM experiments.

Conflicts of Interest: The authors declare no conflict of interest.

References

1. Van der Voort, P.; Vercaemst, C.; Schaubroeck, D.; Verpoort, F. Ordered mesoporous materials at the beginning of the third millennium: new strategies to create hybrid and non-siliceous variants. *Phys. Chem. Chem. Phys.* **2008**, *10*, 347–360. [[CrossRef](#)] [[PubMed](#)]
2. Stein, A.; Melde, B.J.; Schroden, R.C. Hybrid inorganic-organic mesoporous silicates-nanoscope reactors coming of age. *Adv. Mater.* **2000**, *12*, 1403–1419. [[CrossRef](#)]
3. Sayari, A.; Hamoudi, S. Periodic Mesoporous Silica-Based Organic–Inorganic Nanocomposite Materials. *Chem. Mater.* **2001**, *13*, 3151–3168. [[CrossRef](#)]
4. Hatton, B.; Landskron, K.; Whitnall, W.; Perovic, D.; Ozin, G.A. Past, Present, and Future of Periodic Mesoporous Organosilicas. *Acc. Chem. Soc. Res.* **2005**, *38*, 305–312. [[CrossRef](#)] [[PubMed](#)]
5. Vinu, A.; Hossain, K.Z.; Ariga, K. Recent advances in functionalization of mesoporous silica. *J. Nanosci. Nanotechnol.* **2005**, *5*, 347–371. [[CrossRef](#)]
6. Gan, W.Y.; Chiang, K.; Brungs, M.; Amal, R.; Zhao, H. Dense TiO₂ thin film: Photoelectrochemical and photocatalytic properties. *Int. J. Nanotechnol.* **2007**, *4*, 574–587. [[CrossRef](#)]
7. Hoffman, F.; Cornelius, M.; Morell, J.; Froba, M. Periodic Mesoporous Organosilicas (PMOs): Past, Present, and Future. *J. Nanosci. Nanotechnol.* **2006**, *6*, 265–288. [[CrossRef](#)]
8. Grudzien, R.M.; Grabicka, B.E.; Pikus, S.; Jaroniec, M. Periodic Mesoporous Organosilicas with Ethane and Large Isocyanurate Bridging Groups. *Chem. Mater.* **2006**, *18*, 1722–1725. [[CrossRef](#)]
9. Gianotti, E.; Frache, A.; Coluccia, S.; Thomas, J.M.; Maschmeyer, T.; Marchese, L. The identity of titanium centres in microporous aluminophosphates compared with Ti-MCM-41 mesoporous catalyst and titanosilsesquioxane dimer molecular complex: a spectroscopy study. *J. Mol. Catal. A Chem.* **2003**, *204*, 483–489. [[CrossRef](#)]
10. Hu, Y.; Higashimoto, S.; Martra, G.; Zhang, J.L.; Matsuoka, M.; Coluccia, S.; Anpo, M. Local Structures of Active Sites on Ti-MCM-41 and Their Photocatalytic Reactivity for the Decomposition of NO. *Catal. Lett.* **2003**, *90*, 161–163. [[CrossRef](#)]
11. Chao, M.C.; Lin, H.P.; Mou, C.Y.; Cheng, B.W.; Cheng, C.F. Synthesis of nano-sized mesoporous silicas with metal incorporation. *Catal. Today* **2004**, *97*, 81–87. [[CrossRef](#)]
12. Vinu, A.; Ariga, K.; Saravanamurugan, S.; Hartmann, M.; Murugesan, V. Synthesis of highly acidic and well ordered MgAl-MCM-41 and its catalytic performance on the isopropylation of m-cresol. *Microporous Mesoporous Mater.* **2004**, *76*, 91–98. [[CrossRef](#)]
13. Alba, M.D.; Luan, Z.H.; Klinowski, J. Titanosilicate Mesoporous Molecular Sieve MCM-41: Synthesis and Characterization. *J. Phys. Chem.* **1996**, *100*, 2178–2182. [[CrossRef](#)]

14. Morey, M.S.; O'Brien, S.; Schwarz, S.; Stucky, G.D. Hydrothermal and Postsynthesis Surface Modification of Cubic, MCM-48, and Ultralarge Pore SBA-15 Mesoporous Silica with Titanium. *Chem. Mater.* **2000**, *12*, 898–911. [[CrossRef](#)]
15. Zhang, W.; Froba, M.; Wang, J.; Tanev, P.T.; Wong, J.; Pinnavaia, T.J. Mesoporous Titanosilicate Molecular Sieves Prepared at Ambient Temperature by Electrostatic (S^+I^- , $S^+X^-I^+$) and Neutral (S^+I^0) Assembly Pathways: A Comparison of Physical Properties and Catalytic Activity for Peroxide Oxidations. *J. Am. Chem. Soc.* **1996**, *118*, 9164–9171. [[CrossRef](#)]
16. Luan, Z.; Mases, E.M.; van der Heide, P.A.W.; Zhao, D.; Czernuszewicz, R.S.; Kevan, L. Incorporation of Titanium into Mesoporous Silica Molecular Sieve SBA-15. *Chem. Mater.* **1999**, *11*, 3680–3686. [[CrossRef](#)]
17. Zhang, W.H.; Lu, J.; Han, B.; Li, M.; Xiu, J.; Ying, P.; Li, C. Direct Synthesis and Characterization of Titanium-Substituted Mesoporous Molecular Sieve SBA-15. *Chem. Mater.* **2002**, *14*, 3413–3421. [[CrossRef](#)]
18. Ji, G.; Zhao, X.S. Characterization and Photocatalytic Properties of Titanium-Containing Mesoporous SBA-15. *Ind. Eng. Chem. Res.* **2006**, *45*, 3569–3573.
19. Morishita, M.; Shiraishi, Y.; Hirai, T. Ti-Containing Mesoporous Organosilica as a Photocatalyst for Selective Olefin Epoxidation. *J. Phys. Chem. B* **2006**, *110*, 17898–17905. [[CrossRef](#)]
20. Shiraishi, Y.; Morishita, M.; Hirai, T. Acetonitrile-assisted highly selective photocatalytic epoxidation of olefins on Ti-containing silica with molecular oxygen. *Chem. Commun.* **2005**, 5977–5979. [[CrossRef](#)]
21. Anpo, M.; Yamashita, H.; Ikeue, K.; Fujii, Y.; Zhang, S.G.; Ichihashi, Y.; Park, D.R.; Suzuki, Y.; Koyano, K.; Tatsumi, T. Photocatalytic reduction of CO_2 with H_2O on Ti-MCM-41 and Ti-MCM-48 mesoporous zeolite catalysts. *Catal. Today* **1998**, *44*, 327–332. [[CrossRef](#)]
22. Taramasso, M.; Perego, G.; Notari, B. Preparation of Porous Crystalline Synthetic Material Comprised of Silicon and Titanium Oxides. U.S. Patent 4410501, 18 October 1983.
23. Blasco, T.; Comblor, M.A.; Corma, A.; Pariente, J.P. The state of Ti in titanosilicates isomorphous with zeolite beta. *J. Am. Chem. Soc.* **1993**, *115*, 11806–11813. [[CrossRef](#)]
24. Comblor, M.A.; Corma, A.; Martin, A.; Pariente, J.P. Synthesis of a titaniumsilicoaluminate isomorphous to zeolite beta and its application as a catalyst for the selective oxidation of large organic molecules. *Chem. Commun.* **1992**, 589–590. [[CrossRef](#)]
25. Kapoor, M.P.; Raj, A. Synthesis of mesoporous hexagonal titanium aluminophosphate molecular sieves and their catalytic applications. *Appl. Catal.* **2000**, *203*, 311–319. [[CrossRef](#)]
26. Kapoor, M.P.; Bhaumik, A.; Inagaki, S.; Kuraoka, K.; Yazawa, T. Titanium containing inorganic–organic hybrid mesoporous materials with exceptional activity in epoxidation of alkenes using hydrogen peroxide. *J. Mater. Chem.* **2002**, *12*, 3078–3083. [[CrossRef](#)]
27. Kapoor, M.P.; Sinha, A.K.; Seelan, S.; Inagaki, S.; Tsubota, S.; Yoshida, H.; Haruta, M. Hydrophobicity induced vapor-phase oxidation of propene over gold supported on titanium incorporated hybrid mesoporous silsesquioxane. *Chem. Commun.* **2002**, 2902–2903. [[CrossRef](#)]
28. Bhaumik, A.; Kapoor, M.P.; Inagaki, S. Ammoxidation of ketones catalyzed by titanium-containing ethane bridged hybrid mesoporous silsesquioxane. *Chem. Commun.* **2003**, 470–471. [[CrossRef](#)]
29. Ritterskamp, P.; Kuklya, A.; Wustkamp, M.A.; Kerpen, K.; Weidenthaler, C.; Demuth, M. A Titanium Disilicide Derived Semiconducting Catalyst for Water Splitting under Solar Radiation—Reversible Storage of Oxygen and Hydrogen. *Angew. Chem. Int. Ed.* **2007**, *46*, 7770–7774. [[CrossRef](#)]
30. Melero, J.A.; Iglesias, J.; Arsuaga, J.M.; Pardo, J.S.; Frutos, P.d.; Blazquez, S. Synthesis and catalytic activity of organic–inorganic hybrid Ti-SBA-15 materials. *J. Mater. Chem.* **2007**, *17*, 377–385. [[CrossRef](#)]
31. Gunathilake, C.; Jaroniec, M. Mesoporous Organosilica with Amidoxime Groups for CO_2 Sorption. *Appl. Mater. Interfaces* **2014**, *6*, 13069–13078. [[CrossRef](#)]
32. Gunathilake, C.; Gorka, J.; Dai, S.; Jaroniec, M. Amidoxime-modified mesoporous silica for uranium adsorption under seawater conditions. *J. Mater. Chem. A* **2015**, *3*, 11650–11659. [[CrossRef](#)]
33. Gunathilake, C.; Jaroniec, M. Mesoporous alumina–zirconia–organosilica composites for CO_2 capture at ambient and elevated temperatures. *J. Mater. Chem. A* **2015**, *3*, 2707–2716. [[CrossRef](#)]
34. Gunathilake, C.; Gangoda, M.; Jaroniec, M. Mesoporous isocyanurate-containing organosilica–alumina composites and their thermal treatment in nitrogen for carbon dioxide sorption at elevated temperatures. *J. Mater. Chem. A* **2013**, *1*, 8244–8252. [[CrossRef](#)]
35. Kruk, M.; Jaroniec, M.; Sayari, A. Application of Large Pore MCM-41 Molecular Sieves to Improve Pore Size Analysis Using Nitrogen Adsorption Measurements. *Langmuir* **1997**, *13*, 6267–6273. [[CrossRef](#)]

36. Gunathilake, C.; Dassanayake, R.S.; Kalpage, C.S.; Jaroniec, M. Development of Alumina–Mesoporous Organosilica Hybrid Materials for Carbon Dioxide Adsorption at 25 °C. *Materials* **2018**, *11*, 2301. [[CrossRef](#)]
37. Gunathilake, C.; Manchanda, A.S.; Ghimire, P.; Kruk, M.M.; Jaroniec, M. Amine-modified silica nanotubes and nanospheres: Synthesis and CO₂ sorption properties. *Environ. Sci. Nano* **2016**, *3*, 806–817. [[CrossRef](#)]



© 2019 by the authors. Licensee MDPI, Basel, Switzerland. This article is an open access article distributed under the terms and conditions of the Creative Commons Attribution (CC BY) license (<http://creativecommons.org/licenses/by/4.0/>).